Blind-area Elimination in Video Surveillance Systems by WiFi Sensing with Minimum QoS Loss

***Abstract*—Video surveillance systems have demonstrated their great importance in security protection these years. However, due to limited budget, installing cameras in every place of surveillance region is not practical and then blind areas become inevitable. As a result, eliminating blind areas with the lowest cost has become a tough challenge. To the best of our knowledge, this is the first work that fixes the blind spots of video surveillance systems based on WiFi sensing technique. By taking either existing WiFi infrastructure or additional cheap WiFi device as the sensing device, this paper attempts to eliminate blind spots with tiny hardware cost. Moreover, in order to completely fix blind area with minimum loss of video communication QoS, the WiFi sensing device's location boundary that satisfies the above objective is modeled and estimated. To that end, a visitor-disturbed channel model is first derived for precisely describing the inherent relation between the appearance of visitor and the change of wireless channel. Then a location boundary model satisfying both blind-area elimination and QoS maximization is further derived. Based on the derived model, a practical system is designed to estimate the real location boundary. The simulation and experiment results have not only verified the correctness of our derived location boundary model, but also showed its good performance on both blind-area elimination and communication QoS optimization.**

***Index Terms*—Video surveillance systems, blind area, WiFi sensing, communication QoS**

I. Introduction

Video surveillance systems have played an important role in ensuring the safety of people and property. They have been widely deployed in many public and private settings such as office buildings, railway stations, factories and supermarkets. Intelligent video surveillance systems are able to restrain and alert those uninvited visitors who try to damage the safety of people and property in surveillance zone. Due to limited budget, a video surveillance system cannot cover every place of surveillance region. So the existing of blind area is inevitable. Fixing these blind spots with low extra cost is very important for video surveillance systems.

In order to eliminate blind spots with low extra cost, one intuitive idea is deploying additional and cheap devices in the blind spots or beside the blind spots. Many kinds of sensing devices can be used to monitor and detect the appearance of visitors in the blind area, such as acoustic sensor [1], ultrasonic sensor [2], infrared sensor [3] and light sensor [4]. Different from cameras, the above devices cannot capture the image of visitors. But these sensing devices are much cheaper than cameras and able to meet the low-cost requirement for fixing the blind spots. These devices each contain not only a sensing module but also a communication module, because once they detect the appearance of visitors in the blind area, they need to report detection results to the video surveillance systems. More precisely, these sensing devices need to send detection results to the nearest cameras. Hence the communication link between a sensing device and its nearest camera should be established first. The communication can be implemented by practical short-range data communication techniques such as ZigBee [5], Bluetooth [6] and WiFi [7]. Among existing communication techniques, WiFi is the most attractive because of its lowest deployment cost. This is due to the rapid growth and wide deployment of WiFi infrastructure in the past decades. In addition, WiFi has become the preferred choice for wirelessly networking the cameras in video surveillance systems nowadays [7], especially when it is very difficult to connect the cameras by cables in complex environment. As a result, the additional sensing device is supposed to consist of a sensing module and a WiFi communication module.

Since WiFi is employed for the communication between the additional sensing device and its nearest camera, the cost of fixing blind spots can be further minimized by the merging of sensing module and communication module in the sensing device. The mergence can be fulfilled by the technique of WiFi sensing [7]. In the means of WiFi sensing, a cheap WiFi device has the functions of both communication and sensing. So this paper proposes to fix blind spots by WiFi sensing. In practice, the WiFi sensing device can be either an access point or a router in existing WiFi infrastructure, or an additional cheap WiFi module such as ESP-12E [8].

A lot of WiFi sensing methods have been proposed these years. The earliest methods [9], [10] are based on received signal strength (RSS), since RSS can be easily accessed by almost all wireless devices. In those methods, the RSS of WiFi signal is used to passively track moving objects and detect their actions. The rationale behind is that RSS changes with the appearance and movement of the objects near wireless devices. However, as condensing all channel information into a single power value, the RSS characterizes wireless channel in a very coarse manner. So the problem of RSS-based WiFi sensing methods is that their performance is not stable and the sensing range is too short. On the contrary, channel state information (CSI)-based sensing methods have much longer sensing range and much better stability. The reason is that CSI can provide finer and more accurate wireless channel information on multiple subcarriers in the physical layer than RSS. Hence the time-series of CSI amplitude and phase can represent more precisely the channel change caused by the appearance and movement of nearby objects. Although CSI-based sensing methods can achieve good detection accuracy,

the sensing boundary is still missing. However, the investigation on sensing boundary is very important for WiFi sensing methods. The reason is that the derived or measured sensing boundary can not only tell us the longest sensing range of the adopted WiFi sensing method, but also guide us to properly deploy the WiFi sensing devices so that the sensing range can be well extended. If WiFi sensing methods were used to fix blind spots in video surveillance systems, the sensing boundary could guide the deployment of WiFi sensing devices so that the blind areas could be fully eliminated with minimum loss of quality of service (QoS) in video communication.

The main contributions of this paper are summarized as follow.

1. To the best of our knowledge, this is the first work that fixes the blind spots of video surveillance systems based on WiFi sensing technique. By either reusing the existing WiFi infrastructure or deploying additional cheap WiFi device, this paper attempts to eliminate blind spots with extra cost as low as possible. Besides, based on the amplitude of CSI, the simplest but efficient WiFi sensing method is adopted so that the computational complexity can be effectively reduced.

2. For fully covering blind spots with minimum QoS loss, the boundary position of WiFi sensing device is derived. To that end, we first derive a visitor-disturbed channel model for precisely describing the inherent relation between the appearance of visitor and the change of wireless channel. Then we further derive a sensing boundary model which reveals the sensing device's location boundary by satisfying both blind-area elimination and QoS maximization.

3. We propose a practical system to estimate the real location boundary of sensing device. The estimation system is implemented with existing WiFi infrastructure and commodity WiFi devices. Based on the practical system, extensive experiments have been conducted. The experiment results have verified the correctness and effectiveness of our derived boundary model.

II. Related work

A. Blind-zone elimination in video surveillance system

Many methods have been proposed these years to eliminate the blind spots of video surveillance systems. In [11] and [12], the fisheye lens were used as the video acquisition node to obtain the 360 degree panoramic image of the blind area. In [13], six normal lens with the field of view of 65° were used to achieve no blind area monitoring while the neighboring two lens' view fields have an overlap of 5°. In [14], the system first sensed the orientation of child by passive Infrared (PIR) sensors and then rotated the camera by a motor to cover all surveillance areas in the room. In [15], the system integrated acoustic sensor array into the intelligent video monitoring system so that the sound source could be tracked. The above work could only eliminate blind spots in a limited region close to the camera, whereas the blind area further away from the camera could not be eliminated. In [16], ultrasonic sensors were used to measure the approximate position of animals in the forest, while infrared thermal imaging cameras were used to monitor the entry and exit of humans or animals. In [17], the system used an infrared sensor to detect visitor and then called the camera to locate the visitor. In [18], ultrasonic sensor was used to detect the living person and trigger the camera to display the scene. In [19], the system used ultrasonic sensors to detect persons who attempt to invade protected property and the image of the invader was captured by camera. Blind-area elimination based on WiFi sensing was rarely reported.

B. Human detection and tracking based on WiFi sensing

Human detection and tracking based on WiFi sensing have become attractive these years because of the vast deployment of WiFi infrastructure. In [9], the system used a triangulation algorithm based on received signal strength (RSS) to locate persons and counted the people based on the media access control (MAC) address of mobile devices. In [**?**], a vision-based indoor human detection and tracking method was proposed by combining a single static camera and RSS information of WiFi devices. Secure-Pose [20] first extracted retrievable human pose features from video and WiFi CSI streams, then used a detection network to accurately discover forgery attacks and finally devised a localization algorithm to track forgery traces in video streams. Wi2Vi [21] associated variations in the WiFi channel state information with video frames. The system could generate video frames entirely by using CSI measurements and provide auxiliary information to the conventional surveillance system in critical circumstances. In [22], the system deployed a video surveillance system in two scenarios to capture the video stream and synchronized WiFi signal. To achieve indoor monitoring, a deep network based on LSTM was used for event classification and identification. Although the above work used WiFi signals to help tracking and recognizing objects, WiFi sensing was seldom used to eliminate blind spots in video surveillance systems.

III. Visitor-involved WiFi CSI model

Since the basic idea of fixing blind spots via WiFi signal is leveraging the channel change caused by the appearance of visitor, we derive the WiFi channel model influenced by nearby visitor in this section. Then based on the derived channel model, we will derive boundary positions of WiFi sensing device in next section. In this section we first describe multi-path channel model without visitor in blind area, then derive a visitor-involved channel model.

A. Wireless channel without visitor in blind area

In order to completely cover the blind area, the WiFi sensing device is normally deployed inside the blind area. Hence the line-of-sight (LoS) communication path between the sensing device and the nearest camera is usually obstructed by the walls that produce the blind spots. Then the WiFi signal emitted by the sensing device should propagate through non-LoS paths until reaching the nearest camera. Examples of different non-LoS paths are shown in Fig. 1. Observed from Fig. 1, the WiFi signal experiences reflection along each non-LoS path. It is reflected once along some paths and twice along

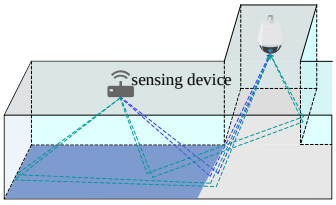

Fig. 1. Example of non-LoS propagation paths covering blind spots

other paths. The paths on which the signal is reflected three times or more are not shown in the figure because the signal should become much weaker if it is reflected multiple times. In the figure, the reflection points of some paths can reach as far as the end of the blind area, so that the blind area is completely covered by the wireless signals.

When a signal originated from the sensing device takes different paths to the destination i.e. the camera, the received signal at the camera is in fact a superposition of signals from many non-LoS paths. Before the superposition, the received signal from each path has much weaker power than the original one. Besides, its phase is also changed at each point of reflection. The above multi-path propagation can be characterized by the following channel impulse response.

$$h(\tau) = \frac{c}{f}\sum_{i=1}^{M}\frac{\prod_{r=1}^{R_i}\varepsilon_r e^{-j\theta_r}}{(4\pi d_i)^{n/2}}\delta\left(\tau-\tau_i\right)+z(\tau), \qquad (1)$$

where τ represents time, c and f are the speed and frequency of electromagnetic wave, respectively, M is the number of all propagation paths, while i is the sequence number of each non-LoS path. On the i-th path, d_i is the distance of the path, n is path loss factor which is more than 2 in indoor environment, τ_i is propagation delay which equals d_i/ c, while R_i is the number of reflection along the path. Upon each reflection, r is the sequence number of the reflection, ε_r is the reflection coefficient [23] and θ_r is the change of phase caused by the reflection. Always smaller than 1, ε_r is related to the reflector of the r-th reflection, e.g. its material. According to the Fresnel equation [24], θ_r is normally either π or 0. When R_i increases, the multiplication of more ε_r together with the increase of d_i should significantly decrease the amplitude of $h(\tau)$ on the i-th path. As a result, R_i is limited to no more than 2. $z(\tau)$ represents the noise from the receiver.

Based on Fourier transform, the above channel impulse response is transformed into corresponding channel frequency response denoted as H_{t,f,a_w,a_c}. The meaning of the four subscript symbols t, f, a_w and a_c is explained as follow. t represents the time period of Fourier transform upon channel impulse response. In practice, t lasts for a short period and proceeds with time, so that the real-time and latest channel frequency response can be obtained. f is the frequency of subcarrier since the channel estimation of WiFi systems has been refined to the granularity of subcarriers. a_w represents the index of a concerned antenna at the WiFi sensing device if the device has more than one antennas, so a_w can tell which antenna is used to send the signal that further contributes the estimation of the channel frequency response. Similarly, a_c is the index of a concerned receiving antenna at the camera. Given a fixed time period t, since the utilized WiFi system has dozens of subcarriers while the sensing device and the camera may have multiple antennas, we can obtain as many as $N_f \times N_{a_w} \times N_{a_c}$ channel frequency responses. Here, N_f, N_{a_w} and N_{a_c} denote the number of subcarriers, antennas at the sensing device and antennas at the camera, respectively. In WiFi systems, the channel frequency response is measured as CSI and the measurements are conducted periodically. If we denote the CSI as C_{k,f,a_w,a_c}, the interval between adjacent measurements as Δt and the duration of one single measurement (i.e. duration of a CSI packet) as t_p, then t is actually the period between $k\Delta t$ and $t_p + k\Delta t$, so we can write C_{k,f,a_w,a_c}=$H_{(k\Delta t,t_p+k\Delta t),f,a_w,a_c}$. Similar to channel frequency response, given a period indexed as k, the single CSI measurement has a dimension of $N_f \times N_{a_w} \times N_{a_c}$. If not reduced, such a high dimension will result in very complex algorithm which is not suitable for resource-constrained WiFi sensing devices. So in order to minimize the computational complexity, the above high dimension will be reduced to one in the practical system proposed in this paper. After dimensionality reduction, the CSI measurement at time index k can be written in short as C_k. Since the channel frequency response is obtained by the Fourier transform upon (1), we have

$$C_k = \frac{c}{f}\sum_{i=1}^{M}\frac{(\prod_{r=1}^{R_{i,k}}\varepsilon_r)e^{-j(2\pi f\tau_{i,k}+\sum_{r=1}^{R_{i,k}}\theta_r)}}{(4\pi d_{i,k})^{n/2}} + Z_k(f), \quad (2)$$

where the subscript k represents the k-th measurement and $Z_k(f)$ is frequency response of the noise at the k-th measurement.

B. Visitor-involved CSI model

The wireless channel model derived in last section was relatively static because no visitor appeared. But when a visitor enters the blind area, the wireless channel (represented by CSI) between the sensing device and the camera should be influenced immediately. The reason is that the appearance of visitor changes some propagation paths of WiFi signal, especially those paths around the visitor.

The change can be categorized into two kinds: obstruction and redirection. As the first kind of change, some propagation paths of WiFi signal are obstructed by the visitor. When there was no visitor, those paths were supposed to go straightway to the expected destination or reflector. But when the visitor exists in the way of those paths, the propagation of WiFi signal will be blocked by the visitor because WiFi signal can hardly go through the body of visitor. Since most part of human body is composed by water, the power loss should be extremely large when WiFi signal propagates through human body [25]. The group of propagation paths obstructed by the visitor is denoted as GP_{obs}. The number of paths in GP_{obs} is denoted as N_{obs}.

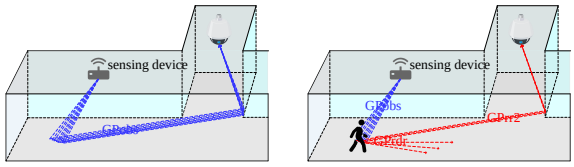

(a) no visitor (b) with visitor

Fig. 2. Example of redirection change

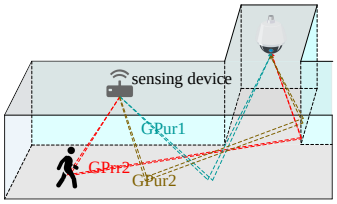

Fig. 3. Example of propagation paths with visitor in the blind area

As the second kind of change, part of the obstructed paths immediately redirect signal propagation. Among all the N_{obs} obstructed paths in GP_{obs}, some of them continue their original direction, so the corresponding signals go into the body of visitor and eventually evaporate because of sharp power loss. On the contrary, the signals on other obstructed paths change their direction. These redirection paths use the visitor as the reflector, so these redirection paths can be regarded as the part of obstructed paths that are reflected via the visitor. If the reflection coefficient of the visitor is denoted as ϵ_{vs}, then according to the meaning of reflection coefficient, the number of redirection paths is calculated as N_{rdr}=$\epsilon_{vs}N_{obs}$. The group of these redirection paths are denoted as GP_{rdr}. On GP_{rdr}, starting from the visitor, the signals are reflected toward many different directions. An example of the kind of redirection change is shown in Fig. 2. When there is no visitor, as depicted in Fig. 2(a), the original direction of the paths GP_{obs} is first toward the ground where occurs the first reflection, then toward the right wall of the right corridor where happens the second reflection and finally toward the camera. Later when a visitor appears in the blind area, the paths in GP_{rdr} which is part of GP_{obs} change their directions, as shown in Fig. 2(b).

Among all the redirection paths in GP_{rdr}, we are only interested in part of them that can reach the camera via one subsequent reflection. The reason is that the number of reflection on each path in channel model has been limited to no more than two, which has been explained in last subsection. These redirection paths with twice-reflection are marked in red in Fig. 2(b). These paths can either take the ground or the right wall as the second reflector. We denote this group of redirection paths with twice-reflection as GP_{rr2}, while the number of paths in GP_{rr2} is denoted as N_{rr2}. Obviously GP_{rr2} is part of GP_{rdr} and N_{rr2} is less than N_{rdr}. The more precise relation between N_{rr2} and N_{rdr} depends on real space structure of the whole surveillance region.

From the above analysis, the propagation paths of WiFi signal with visitor can be classified into three types: once-reflection paths unrelated with visitor, twice-reflection paths unrelated with visitor and twice-reflection paths related with visitor. In fact, the third type of paths has just been denoted as GP_{rr2}. We then denote the first type of paths as GP_{ur1} and the number of paths in GP_{ur1} as N_{ur1}. The second type of paths is denoted as GP_{ur2} and the number of paths in GP_{ur2} is N_{ur2}. These three types of paths are also shown in Fig. 3.

Since the propagation paths in visitor scenario have been divided into three types, accordingly the CSI model in visitor scenario can also be divided into three parts. The three parts of CSI are denoted as $C_{k,ur1}$, $C_{k,ur2}$ and $C_{k,rr2}$, respectively, corresponding to the three types of paths. Then based on (2), the visitor-involved CSI model can be expressed as

$$C_k = C_{k,ur1} + C_{k,ur2} + C_{k,rr2} + Z_k(f), \tag{3}$$

where

$$C_{k,ur1} = \frac{c}{f}\sum_{i=1}^{N_{ur1}} \frac{\varepsilon_{ur} e^{-j(2\pi f \tau_{i,k}+\theta_{ur})}}{(4\pi d_{i,k})^{n/2}}, \tag{4}$$

$$C_{k,ur2} = \frac{c}{f}\sum_{i=N_{ur1}+1}^{N_{ur1}+N_{ur2}} \frac{\varepsilon_{ur}^2 e^{-j(2\pi f \tau_{i,k}+2\theta_{ur})}}{(4\pi d_{i,k})^{n/2}}, \tag{5}$$

$$C_{k,rr2} = \frac{c}{f}\sum_{i=N_{ur1}+N_{ur2}+1}^{N_{ur1}+N_{ur2}+N_{rr2}} \frac{\varepsilon_{vs}\varepsilon_{ur} e^{-j(2\pi f \tau_{i,k}+\theta_{vs}+\theta_{ur})}}{(4\pi d_{i,k})^{n/2}}, \tag{6}$$

ε_{ur} and θ_{ur} are reflection coefficient and phase change at ground or wall, respectively, since ground and wall have similar material, while ε_{vs} and θ_{vs} are reflection coefficient and phase change at the visitor.

IV. Sensing Device Location Boundary Model with Blind-Area Elimination and QoS Maximization

If this paper is only concerned with the effect of blind-area elimination, the sensing device should be placed closest to the key point of the blind area i.e. the entrance of the blind area, because by this placement the visitor can induce the most significant change in wireless channel when it attempts to enter the blind area. However, requiring the placement of sensing device at the blind entrance should raise several issues. Two major issues are explained as follow. The first and most important issue is deteriorating the quality of service (QoS) of communication between the sensing device and the nearest camera. The reason is that when the sensing device gets closer to the blind entrance, meanwhile it goes further away from the camera, then the longer distance between the sensing device and the camera should worsen their communication quality, e.g. increasing packet loss and raising power consumption [**?**], [20]. This issue is particularly important when the sensing device happens to be WiFi infrastructure (e.g. AP or router) because the communication quality between WiFi infrastructure and the camera has dominant influence on the video

transmission data rate and stability. The second issue is losing space freedom of device placement. In real scenario there may be no available place to deploy the sensing device at the blind entrance. Too inflexible limitation on the place may increase the difficulty and cost of the sensing device installation.

Due to the above issues, the sensing device is recommended to be placed not at the entrance of blind area, but at a position that can achieve a balance between blind-area elimination and communication quality. This balanced position is defined as sensing device location boundary. A model for this boundary will be derived in this section. Specifically, we will first formulate the problem of balancing blind-area elimination and communication quality, then solve the problem and meanwhile derive a sensing device location boundary model.

A. Problem formulation

The purpose of formulating an optimization problem is to achieve a balance between blind-area elimination and communication quality. Since the entrance of blind area is usually further away from the camera than other parts of blind area, the pursuit of the best blind-area elimination is always contradictory to the best communication quality of the camera. From the aspect of sensing device location, better blind-area elimination requires the geographical proximity of the sensing device to the blind entrance, which meanwhile pushes the sensing device further away from the camera and thus worsen the communication quality between the sensing device and the camera.

Maximizing the performance on both blind-area elimination and communication quality is not practical, because one optimization problem cannot keep two optimization objectives. Instead, we can put one in the objective and another in the constraint. For blind-area elimination, the basic requirement is that the sensing device should be capable to detect the appearance of visitor when it exists at the front of the blind area. So we take this requirement on blind-area elimination as the constraint in optimization problem. On the other hand, higher QoS including higher data rate and better stability is always the need in video surveillance systems. Hence the maximization of communication quality is taken as the objective. As a result, the optimization problem can be formulated as

$$\max_{P_{sd}} \text{QoS}(P_{cm}, P_{sd}),\ \text{s.t. BCR}(P_{sd}) \geq \text{dis}(P_{sd}, P_{he}), \quad (7)$$

where the function QoS represents the communication quality (e.g. channel quality, data rate) between sensing device and the nearest camera, the function of blind-clear range (BCR) represents how far in the blind area the sensing device's sensing range can reach, while the function dis represents the distance between two positions. P_{sd}, P_{cm} and P_{he} represent the positions of the sensing device, the nearest camera and the visitor at the blind entrance. When the constraint is satisfied, the blind entrance is covered in the sensing range, then the entire blind area is supposed to be fixed since the blind entrance cannot be bypassed by the visitor.

Since the communication QoS between the sensing device and the camera increases with the closeness between P_{sd} and P_{cm}, meanwhile the QoS should increase with the distance between P_{sd} and P_{he}. So (7) is equivalent to

$$\max_{P_{sd}} \text{dis}(P_{sd}, P_{he}),\ \text{s.t. BCR}(P_{sd}) \geq \text{dis}(P_{sd}, P_{he}). \quad (8)$$

If the sensing device is too far away from the blind entrance, the sensing range can hardly cover the blind entrance. When dis(P_{sd}, P_{he}) gets smaller, the sensing range of the sensing device approaches the blind entrance, i.e., the sensing range reaches further and covers more blind area. So BCR(P_{sd}) increases with the decrease of dis(P_{sd}, P_{he}). Since (8) aims to obtain the maximum distance, the objective is equivalent to minimizing BCR. So (8) can be converted to finding the P_{sd} that satisfies

$$\text{BCR}(P_{sd}) = \text{dis}(P_{sd}, P_{he}). \quad (9)$$

B. Problem materialization by a low-complexity amplitude-based sensing method

In order to materialize BCR, we need to obtain specific expression of the sensing range of WiFi sensing device. The sensing range depends on practical sensing method employed by the sensing device. Although many WiFi sensing methods have been proposed these years, we prefer low-complexity sensing methods because low-cost sensing devices and cameras do not possess powerful resources to execute complex algorithms. Hence a simple sensing method based on the amplitude of CSI is used in this paper.

The main idea of the amplitude-based sensing method is explained as follow. When there is no visitor, the amplitude of measured CSI is recorded as $A(C_0)$. Here the subscript 0 represents the initial time point. Before the appearance of visitor, the whole surveillance area keeps relatively static as well as the channel between the sensing device and the camera, so $A(C_0)$ also keeps unchanged until the arrival of visitor. When the visitor exists in the blind area, the amplitude of CSI should be changed. The position of visitor is denoted as P_{vs} and the amplitude of current CSI is recorded as $A(C_{vs})$. At this time point, the change can be represented as ΔC_{vs}=$abs(A^2(C_{vs}) - A^2(C_0))$. For the ease of later expansion of the above expression, the square of amplitude is used in the above expression instead of amplitude itself. The change ΔC_{vs} grows gradually as the visitor gets closer to the sensing device, because the approaching of visitor makes greater influence on the wireless channel. When ΔC_{vs} grows big enough, the appearance of the visitor is supposed to be sensed by the sensing device. For lowest possible computational complexity, a threshold denoted as δ_C is set here to judge whether ΔC_{vs} is big enough or not. Therefore, given the position of the sensing device, its sensing range in the form of BCR can be formulated as

$$\text{BCR}(P_{sd}) = \max_{P_{vs}} \text{dis}(P_{sd}, P_{vs}),\ \text{s.t. } \Delta C_{vs} \geq \delta_C. \quad (10)$$

Since ΔC_{vs} grows with the decrease of dis(P_{sd}, P_{vs}), the sensing range is actually the distance between P_{sd} and the

furthest position of the visitor that can be detected by the sensing device. So (10) is equivalent to

$$\text{BCR}(P_{sd}) = \text{dis}(P_{sd}, P_{vs}),\ \text{s.t. } \Delta C_{vs} = \delta_C. \quad (11)$$

Combining (9) and (11), the optimization problem can be converted to finding the P_{sd} that satisfies

$$\text{BCR}(P_{sd}) = \text{dis}(P_{sd}, P_{he}),\ \text{s.t. } \Delta C_{he} = \delta_C. \quad (12)$$

C. Derivation of sensing device location boundary model

Combining the above problem with the previous channel model, in this subsection we derive a model of sensing device location boundary. First, according to the expression of ΔC_{he}, the constraint in (12) is actually

$$abs(A^2(C_{he}) - A^2(C_0)) = \delta_C, \quad (13)$$

where C_{he} is the CSI when the visitor locates at the blind entrance.

According to (3), C_{he} is expressed as

$$C_{he} = C_{he,ur1} + C_{he,ur2} + C_{he,rr2} + Z_{he}, \quad (14)$$

where

$$C_{he,ur1} = \frac{c}{f}\sum_{i=1}^{N_{ur1}} \frac{\varepsilon_{ur} e^{-j(2\pi f \tau_{i,he} + \theta_{ur})}}{(4\pi d_{i,he})^{n/2}}, \quad (15)$$

$$C_{he,ur2} = \frac{c}{f}\sum_{i=N_{ur1}+1}^{N_{ur1}+N_{ur2}} \frac{\varepsilon_{ur}^2 e^{-j(2\pi f \tau_{i,he} + 2\theta_{ur})}}{(4\pi d_{i,he})^{n/2}}, \quad (16)$$

$$C_{he,rr2} = \frac{c}{f}\sum_{i=N_{ur1}+N_{ur2}+1}^{N_{ur1}+N_{ur2}+N_{rr2}} \frac{\varepsilon_{vs}\varepsilon_{ur} e^{-j(2\pi f \tau_{i,he} + \theta_{vs} + \theta_{ur})}}{(4\pi d_{i,he})^{n/2}}. \quad (17)$$

Then according to (2), C_0 is expressed as

$$C_0 = \frac{c}{f}\sum_{i=1}^{M} \frac{(\prod_{r=1}^{R_{i,0}} \varepsilon_r) e^{-j(2\pi f \tau_{i,0} + \sum_{r=1}^{R_{i,0}} \theta_r)}}{(4\pi d_{i,0})^{n/2}} + Z_0. \quad (18)$$

Similar to (14), the paths in (18) can also been divided into three parts. Comparing Fig. 3 with Fig. 1, we can find the following relation between the paths in C_{he} and C_0. First, the paths GP_{ur1} i.e. from the 1st path to the N_{ur1}-th path in C_{he} (shown in Fig. 3) come from all the once-reflection paths in C_0 (shown in Fig. 1). Second, the paths GP_{ur2} i.e. from the $(N_{ur1}+1)$-th to the $(N_{ur1}+N_{ur2})$-th path in C_{he} are from part of twice-reflection paths in C_0. Third, the other part of twice-reflection paths in C_0 are first blocked by the visitor, then redirected and some of the redirected paths become GP_{rr2}. So the number of paths in the other part of twice-reflection paths in C_0 can be calculated as $N_{or2} = N_{rr2}/(\varepsilon_{vs}\eta_{rr})$, where η_{rr} denotes the ratio of N_{rr2} to all the redirected twice-reflection paths. Summarizing the above three aspects of relation, we can rewrite C_0 as

$$C_0 = C_{he,ur1} + C_{he,ur2} + C_{0,or2} + Z_0, \quad (19)$$

where

$$C_{0,or2} = \frac{c}{f}\sum_{i=N_{ur1}+N_{ur2}+1}^{N_{ur1}+N_{ur2}+N_{or2}} \frac{\varepsilon_{ur}^2 e^{-j(2\pi f \tau_{i,0} + 2\theta_{ur})}}{(4\pi d_{i,0})^{n/2}}. \quad (20)$$

From (14) and (19), C_{he} can be rewritten as

$$C_{he} = C_{he,rr2} + (C_0 - C_{0,or2}) + (Z_{he} - Z_0). \quad (21)$$

For the same receiver, the frequency response of noise is assumed to stable with time, so $Z_{he} - Z_0$ can be removed. Since C_0 is obtained in the scenario of no visitor, $C_0 - C_{0,or2}$ has no relation with the visitor. So in the above equation, only $C_{he,rr2}$ is related with the visitor and it can be regarded as a function of the three positions P_{sd}, P_{he} and P_{cm}.

Since C_{he} is a complex value, its real part and imaginary part can be expressed as

$$\text{Re}(C_{he}) = \text{Re}(C_{he,rr2}) + \text{Re}(C_0 - C_{0,or2}) \quad (22)$$

and

$$\text{Im}(C_{he}) = \text{Im}(C_{he,rr2}) + \text{Im}(C_0 - C_{0,or2}), \quad (23)$$

respectively. Then the square of amplitude of C_{he} can be calculated as

$$A^2(C_{he}) = J(P_{sd}, P_{he}, P_{cm}) + A^2(C_0 - C_{0,or2}), \quad (24)$$

where the function $J(P_{sd}, P_{he}, P_{cm})$ is

$$J = A^2(C_{he,rr2}) + \alpha\text{Re}(C_{he,rr2}) + \beta\text{Im}(C_{he,rr2}), \quad (25)$$

$\alpha = 2\,\text{Re}(C_0 - C_{0,or2})$, $\beta = 2\,\text{Im}(C_0 - C_{0,or2})$.

With (24) substituted into (13), the location boundary of sensing device that balances blind-area elimination and QoS turns to be the P_{sd} that satisfies

$$(J(P_{sd}, P_{he}, P_{cm}) + A^2(C_0 - C_{0,or2}) - A^2(C_0))^2 = \delta_C^2. \quad (26)$$

V. Sensing device location boundary estimation system with balanced blind-area elimination and QoS

Although numeric results of sensing device location boundary can be simulated by the derived boundary model, the correctness and effectiveness of the derived model should be verified by a prototype system. Therefore, in order to estimate the real location boundary with balanced blind-area elimination and QoS, a prototype system is designed in this section. For lowest possible computational complexity, the system utilizes the amplitude-based sensing method in last section. Besides, the high dimension of orignal CSI data is significantly reduced, while the most useful information embedded in the data is retained.

The main procedure of the system is briefly introduced as follow. The sensing device is moved at a short step in the direction away from the blind entrance. When the sensing device stops at each location, it executes the following four-step sensing method. The first step is using filters to eliminate the outliers and noise in original CSI measurements. The second step is recording the initial CSI in the case of no visitor and later recording the CSI as the visitor appears at the blind

entrance. The third step is calculating the change of CSI at all subcarriers and all antenna-pairs and then selecting the largest one. The fourth step is judging whether the visitor is detected based on the difference between the change of CSI and a preset threshold. The sensing device moves and repeating the above four steps until the difference between the change of CSI and a preset threshold is small enough. The above procedure is illustrated in detail as follows.

At the first step, in the amplitude of original CSI measurements, outliers are removed and noise is reduced. To effectively eliminate the outliers caused by burst interference of WiFi signals, we use a low-complexity method i.e. Hampel identifier [26]. Then by using a wavelet-based low-pass filter, the noise produced at the receiver is filtered out and the filtered CSI amplitude becomes more clean and smooth.

At the beginning of the second step, since no visitor appears at the very beginning, the filtered amplitude of CSI is recorded as $A(C_0)$. Right now the dimension of CSI amplitude is still as high as $N_f \times N_{a_w} \times N_{a_c}$. If N_f, N_{a_w} and N_{a_c} is respectively 30, 3 and 1, there are as many as 90 amplitude values in this single and initial measurement of CSI. Then once the visitor appears at the entrance of the blind area, the amplitude of CSI is recorded as $A(C_{he})$. It has the same dimension as $A(C_0)$.

At the third step, as adopted in the derived model, the difference between $A(C_{he})$ squared and $A(C_0)$ squared, i.e. $abs(A^2(C_{he}) - A^2(C_0))$ is calculated as the change of CSI. This change of CSI has as many as $N_f \times N_{a_w} \times N_{a_c}$ values. These different values are caused by the frequency-fading and spatial-diversity effects in the wireless channel between the sensing device and the camera. Among all these values, the largest one is selected as the final change of CSI.

At the fourth step, we first compare the aforementioned change of CSI with a preset threshold. The change of CSI should be much bigger than the threshold when the sensing device is placed very close to the blind entrance. Then we move the sensing device away from the blind entrance. At each location of the sensing device, we repeat the above four steps and calculate the difference between the latest change of CSI and the threshold. When the above difference is 0, the boundary location of sensing device is supposed to be found according to our previously derived model. Since the above difference can hardly become exact 0 in real scenario, we replace the requirement of exact 0 by the smallest absolute difference between the change of CSI and the preset threshold. In fact, the smallest absolute difference usually appears when the difference turns from a positive value to a negative value. Finally, the sensing device's location boundary that balances blind-area elimination and QoS is estimated as the sensing device's position where the absolute difference between the change of CSI and the preset threshold is smallest.

VI. Performance Evaluation via Simulation and Experiment

In this section, we first simulate the derived location boundary model and evaluate the performance on both blind-area elimination and QoS according to the simulation results. Then the experiment is conducted based on the designed prototype system. By comparing the experiment results with simulation results, we not only evaluate the real performance of the designed system, but also verify the effectiveness of the derived model.

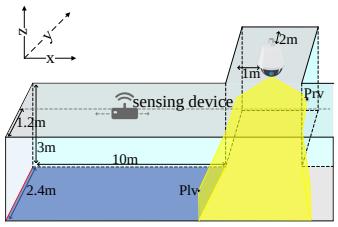

Fig. 4. Simulation scenario of intrusion detection bound

Since the entrance of blind area usually exhibits in the form of a line which we name as blind entrance line, the performance metric of blind-area elimination is set to blind entrance fixed ratio (abbr. BEFR) which is calculated as the ratio of the part of blind entrance line inside sensing range to the entire blind entrance line. For the convenience of comparison with blind-area elimination, the communication QoS between the WiFi sensing device and the camera is evaluated via a strong-related parameter i.e. the proximity between them (abbr. $prx_{sd,cm}$). It is calculated as the inverse of the distance between the sensing device and the camera.

The scenario for both simulation and experiment comes from a real surveillance situation. As shown in Fig. 4, the whole region consists of a horizontal corridor and a vertical corridor. The camera is placed on the ceiling center of the vertical corridor. The distance between the camera and the left wall of the vertical corridor is 1 m, while the distance between the camera and the back wall of the vertical corridor is 2 m. The length, width and height of the horizontal corridor is 10 m, 2.4 m and 3 m, respectively. The field of view of the camera is marked in yellow, while the blind area is marked in blue. The boundary point of the field of view on the middle line of the frontal wall is denoted as P_{lv}, while the boundary point of the field of view on the middle line of the right wall is denoted as P_{rv}. The entrance of the blind area is at the left-most end of the horizontal corridor and is marked in a red line. The sensing device is placed on the ceiling of the horizontal corridor and along the center line of the ceiling. The origin is set at the bottom left of the blind entrance.

A. Evaluation based on simulation results

The values of key simulation parameters in previously derived model are given in Table I. The center frequency of WiFi signal is 2.4 GHz supported by most commercial WiFi devices. The path loss factor n is set to 3 because of indoor propagation scenario. $\varepsilon_{\mathrm{vs}}$ and $\varepsilon_{\mathrm{ur}}$ are estimated based on the permittivity and reflectivity to electromagnetic wave on human and construction, respectively. The phase change is estimated based on the Fresnel equation. The function dis

returns the distance of the path that connects the points of function parameters.

TABLE I
KEY SIMULATION PARAMETERS IN LOCATION BOUNDARY MODEL

Parameter	Value
WiFi frequency	2.4GHz
n	3
$\varepsilon_{\mathrm{ur}}, \varepsilon_{\mathrm{vs}}$	0.38, 0.75
$\theta_{\mathrm{ur}}, \theta_{\mathrm{vs}}$	π
η_{rr}	0.5
d_i in (15)	dis(P_{sd}, P_{lv}, P_{cm})
d_i in (16) and (20)	dis$(P_{sd}, P_{lv}, P_{rv}, P_{cm})$
d_i in (17)	dis$(P_{sd}, P_{he}, P_{lv}, P_{cm})$

Based on the previously derived model, we simulate theoretical sensing device location boundary that aims to maximize communication quality and meanwhile satisfies blind-area elimination. The simulation results under a given δ_C i.e. 10^{-5} are shown in Fig. 5. The communication quality performance represented by the metric $prx_{sd,cm}$ is exhibited in Fig. 5(a), while the blind-area elimination performance represented by the metric BEFR is shown in Fig. 5(b). Since the visitor can enter the blind area from different points of the blind entrance line, the horizontal axis in the figure represents the position of visitor by the distance between the origin and the visitor. The visitor is supposed to locate at six different points along the blind entrance line.

Fig. 5(a) shows how $prx_{sd,cm}$ changes with the visitor's position (i.e. visitor's y-axis coordinate y_{he} since x_{he} is always 0). It can be observed that $prx_{sd,cm}$ decreases as the visitor gets further away from the origin. This phenomenon is equivalent to the increase of dis(P_{sd}, P_{cm}) with y_{he}, since $prx_{sd,cm}$ is the inverse of dis(P_{sd}, P_{cm}). The reason for the phenomenon is explained as follow. When the visitor moves along the blind entrance line and goes further away from the origin, its distance to the reflection point P_{lv} gets larger. The distance of each twice-reflection path via the visitor also becomes larger, since it is approximately equal to the distance of the path that connects the four points P_{sd}, P_{he}, P_{lv} and P_{cm}. This increase of the distance of twice-reflection paths means that the visitor is further away from the wireless channel between the sensing device and the camera. So the visitor has weaker influence on the CSI. The change of CSI has become smaller. Then in order to satisfy the constraint in (13), we need to enlarge the change of CSI by shortening the distance between the visitor and the sensing device. The most effective way is placing the sensing device closer to the visitor. So the sensing device is placed nearer to the blind entrance and meanwhile it is further away from the camera. Hence dis(P_{sd}, P_{cm}) becomes larger, then $prx_{sd,cm}$ becomes smaller. From the above explanation, we can find that although the visitor is always on the entrance line, the specific position of the visitor has considerable influence on the placement of the sensing device for meeting the requirement of blind-area elimination. The placement of sensing device further influences the QoS of its communication with the camera.

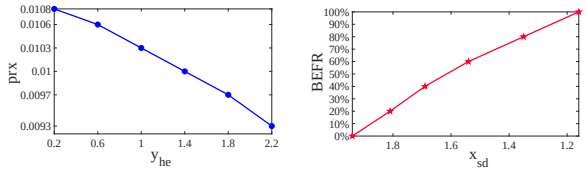

(a) $prx_{sd,cm}$ changes with y_{he} (b) BEFR changes with x_{sd}

Fig. 5. Performance simulation of $prx_{sd,cm}$ and BEFR

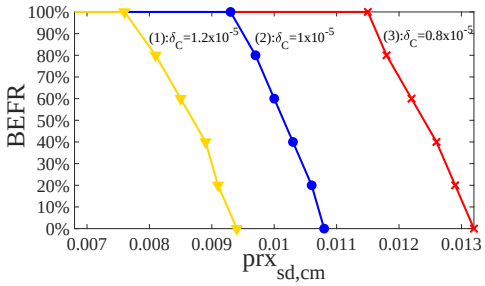

Fig. 6. Simulation results on the relation between performance metrics

Fig. 5(b) shows how the placement of sensing device influences the BEFR. Moving along the middle line of the ceiling in the horizontal corridor, the sensing device keeps its y-axis coordinate unchanged. So in the figure we use the x-axis coordinate to represent the placement of sensing device. It can be observed that the BEFR increases as the sensing device is placed closer to the blind entrance. The observation is explained as follow. When the sensing device gets closer to the blind entrance, more part of the blind entrance line will be covered by the sensing range. So the BEFR increases with the approaching of the sensing device to the blind entrance.

Simulation results on the relation between BEFR and $prx_{sd,cm}$ are shown in Fig. 6. It can be observed that given a threshold, the BEFR generally decreases with $prx_{sd,cm}$. The reason is explained as follow. As illustrated in Fig. 5(b), the BEFR normally decreases with the distance between the sensing device and the blind entrance. Accordingly, since $prx_{sd,cm}$ increases with the above distance, the BEFR should decreases with the growth of $prx_{sd,cm}$. On each curve in Fig. 6, we can also observe the flat part corresponding to 100% BEFR. On the flat part of 100% BEFR, the end point with the the largest $prx_{sd,cm}$ signifies the sensing device's place furthest away from the blind entrance on the condition of complete blind-area elimination. It can also be observed that a smaller δ_C helps pushing the above end point of 100% BEFR toward greater $prx_{sd,cm}$ i.e. better communication QoS. However, the threshold cannot be too smaller, otherwise the sensing device is too far away from the blind entrance that the visitor cannot be detected timely.

B. Evaluation based on experiment results

The experiment scenario is the same as that in Fig. 4. The sensing device is a commercial WiFi router, while the camera is enabled with WiFi functionality but embedding a Intel 5300

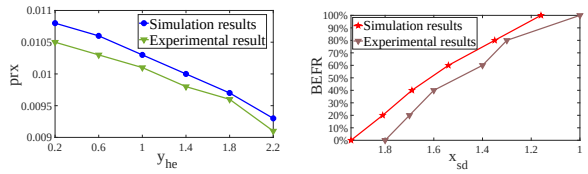

(a) $prx_{sd,cm}$ changes with y_{he} (b) BEFR changes with x_{sd}

Fig. 7. Comparison between experiment and simulation results under given δ_C

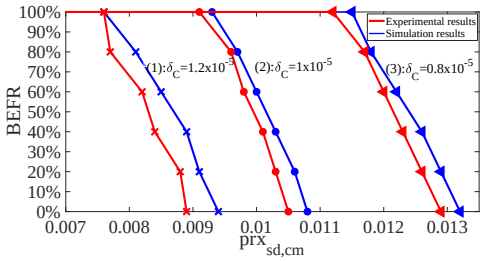

Fig. 8. Experiment results on the relation between performance metrics

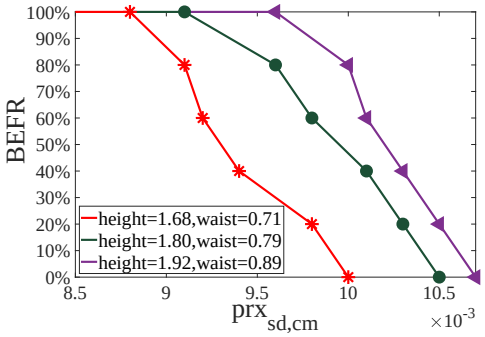

Fig. 9. Experiment results with different sizes of visitor

NIC. The CSI tool in [20] is used to obtain CSI measurements every 0.01 s. The previously designed prototype system is used to process the CSI measurements and estimate real location boundary of sensing device.

The experiment results on the performance of $prx_{sd,cm}$ and BEFR are shown in Fig. 7. The performance data is generated based on the sensing device's real location boundary estimated by the designed system. The simulation results are also given in the figure. The threshold δ_C is set to 10^{-5}. From the comparison between experiment and simulation results in Fig. 7(a), it can be found that at each position of the visitor the simulated $prx_{sd,cm}$ is very close to the real value. Since $prx_{sd,cm}$ is directly calculated based on the boundary location of the sensing device, the above evident proximity between simulated $prx_{sd,cm}$ and the real value demonstrates the correctness and effectiveness of our previously derived sensing device location boundary model. In Fig. 7(b), the similarity between the simulated BEFR and the real performance can also verify the effectiveness of our derived model. Besides, it can be observed that at each position of sensing device, the practical performance on BEFR is always better than the simulated performance. This phenomenon is in fact favorable for practical application of our derived model. The reason is explained as follow. The simulated BEFR is obtained based on our previously derived location boundary model. In practice when the derived model is used to tell us where to place the sensing device, we first set a desired BEFR, convert it to the constraint in the model and finally obtain a boundary location of the sensing device according to the model. So it is the simulated BEFR that equals the desired BEFR when the sensing device is placed at that boundary location. Since the simulated BEFR is found to be smaller than the real BEFR, the real BEFR should be better than the desired one. Therefore that the utilization of our derived location boundary model can help us to achieve even better blind-area elimination performance in practice. So the above phenomenon is advantageous for our derived model.

When the threshold δ_C takes different values, the experiment results on the relation between BEFR and $prx_{sd,cm}$ are shown in Fig. 8. It can be observed that for the same threshold, the real BEFR generally decreases with $prx_{sd,cm}$, similar to the phenomenon in simulation results. It signifies that we cannot maximize the performance of both blind-area elimination and communication QoS. Instead, trade-off between them can be made. For example, if the blind entrance is required to be 100% covered by the sensing range of the sensing device, we can set the BEFR to 100% as the condition and then select the highest $prx_{sd,cm}$ under that condition. From Fig. 8, it can also be observed that when the threshold δ_C changes, the simulation results are always close to the experiment results. It demonstrates the effectiveness of our derived location boundary model in different threshold settings. Besides, the threshold value also influences the trade-off between BEFR and $prx_{sd,cm}$. If the threshold is too small, the sensing device will be placed too far away from the blind entrance, then the blind area may not be completely fixed. But if the threshold is too big, the sensing device should be placed too far away from the camera, then the communication QoS will be damaged. The value of threshold should be decided according to the practical requirement of users.

The influence on the performance by the size of visitor is also investigated. In the experiment we ask three volunteers with different and typical sizes to act the visitor at the blind area entrance. The visitor with the biggest size has a height of 1.92 m and a waist of 0.89 m. The visitor with the second biggest size has a height of 1.80 m and a waist of 0.79 m. The visitor with the third biggest size has a height of 1.68 m and a waist of 0.71 m. Their experiment results on the relation between BEFR and $prx_{sd,cm}$ are shown in Fig. 9. It can be observed that when the visitor has larger size, the boundary location of the sensing device can be pushed closer to the camera on the condition of the same BEFR performance. The reason is that when the visitor stands at the same position, a larger size of the visitor should obstruct more propagation paths of WiFi signal from the nearby sensing device, then has larger influence on the change of CSI. Thus the sensing device

has to be placed further away from the visitor for meeting the requirement on the same BEFR. However, in practice since the size of visitor is unknown in advance, the assumption of visitor with the smallest size is necessary in system design so that the system can keep good robustness on blind-area elimination.

VII. Conclusion

In this paper, we have made the initial attempt to eliminate blind areas of video surveillance systems based on WiFi sensing technique. The existing WiFi infrastructure and cheap WiFi device are used as the sensing device so that the hardware cost is well reduced. In order to completely fix blind spots with minimum cost in the loss of video communication QoS, a location boundary model of sensing device is built and accordingly a practical estimation system is designed. For building the location boundary model, a visitor-involved channel model is first derived so that the inherent relation between the appearance of visitor and the change of wireless channel is precisely described. Based on the channel model, a location boundary model which satisfies both blind-area elimination and communication QoS maximization is derived. Then based on the location boundary model, a practical system is proposed to estimate the real boundary. Together with simulation results, the extensive experiment results have verified the correctness and effectiveness of the derived location boundary model. The results have also demonstrated the balanced performance of the designed system on both blind-area elimination and communication quality optimization.

References

[1] S. Pleshkova and K. Panchev, "Capturing and transferring of acoustic information in a closed room via wireless acoustic sensor network," in *2021 12th National Conference with International Participation (ELECTRONICA)*, 2021, pp. 1–5.

[2] A. Huang, M. Yoshida, Y. Ono, and S. Rajan, "Continuous measurement of arterial diameter using wearable and flexible ultrasonic sensor," in *2017 IEEE International Ultrasonics Symposium (IUS)*, 2017, pp. 1–4.

[3] C. Liu and J. Huang, "Technical analysis on the pyroelectric infrared sensor in intrusion detection devices," in *2017 32nd Youth Academic Annual Conference of Chinese Association of Automation (YAC)*, 2017, pp. 991–994.

[4] H.-Y. Tsai, F.-C. Su, C.-H. Chou, Y.-H. Lin, K.-C. Huang, Y.-J. J. Yang, L.-W. Kuo, L.-D. Liao, and H.-S. Yu, "Wearable inverse light-emitting diode sensor for measuring light intensity at specific wavelengths in light therapy," *IEEE Transactions on Instrumentation and Measurement*, vol. 68, no. 5, pp. 1561–1574, 2019.

[5] M. Zhang and Q. Hu, "A hybrid network smart home based on zigbee and smart plugs," in *2017 7th International Conference on Communication Systems and Network Technologies (CSNT)*, 2017, pp. 389–392.

[6] K.-C. Peng and J.-H. Lee, "A low-cost vital-sign sensor based on bluetooth system," in *2020 IEEE International Conference on Consumer Electronics - Taiwan (ICCE-Taiwan)*, 2020, pp. 1–2.

[7] D. Grzechca, T. Wróbel, and P. Bielecki, "Indoor location and idetification of objects with video survillance system and wifi module," in *2014 International Conference on Mathematics and Computers in Sciences and in Industry*, 2014, pp. 171–174.

[8] R. Morales-Caporal, A. S. Reyes-Galaviz, J. Federico Casco-Vásquez, and H. P. Martínez-Hernández, "Development and implementation of a relay switch based on wifi technology," in *2020 17th International Conference on Electrical Engineering, Computing Science and Automatic Control (CCE)*, 2020, pp. 1–6.

[9] J. Cao, Y. Wang, X. Zhang, X. Sun, and W. Zhao, "Algorithm of moving object detection of surveillance video combined with wifi technology," in *2018 IEEE International Conference on Information and Automation (ICIA)*, 2018, pp. 1582–1586.

[10] Y. Xu, G. Xu, C. Wang, Y. Cheng, and X. Li, "The design of the tracking system base on visual and wireless location appliance," in *2017 29th Chinese Control And Decision Conference (CCDC)*, 2017, pp. 7785–7790.

[11] J. jian Dai and W. bo Han, "Design of no blind area perimeter intrusion recognition system based on fisheye lens," in *International Symposium on Photoelectronic Detection and Imaging 2013: Imaging Sensors and Applications*, J. Ohta, N. Wu, and B. Li, Eds., vol. 8908, International Society for Optics and Photonics. SPIE, 2013, pp. 306 – 312. [Online]. Available: https://doi.org/10.1117/12.2033138

[12] J. H. Wu, G. Y. Zhang, L. Y. Guo, and S. Yuan, "Study the fisheye staring video surveillance system of nothing blind-zone based on the davinci chip," in *Advances in Mechatronics, Automation and Applied Information Technologies*, ser. Advanced Materials Research, vol. 846. Trans Tech Publications Ltd, 2 2014, pp. 574–577.

[13] J. Wu, N. Zhang, G. Zhang, and L. Guo, "Study of the intelligent video surveillance system based on the staring ommateum model," in *Photonics and Optoelectronics Meetings (POEM) 2011: Optoelectronic Sensing and Imaging*, P. Galarneau, X. Liu, and P. Li, Eds., vol. 8332, International Society for Optics and Photonics. SPIE, 2012, pp. 184 – 190. [Online]. Available: https://doi.org/10.1117/12.918732

[14] S. Sundar, R. Ghosh, and H. Shahil, "A prototype of automated child monitoring system," *International journal of computational intelligence research*, vol. 13, no. 7, pp. 1593–1603, 2017. [Online]. Available: http://dx.doi.org/

[15] L. Li, Y. Li, Y. Su, and H. Yu, "Design and implementation of acoustic localization in intelligent video surveillance system," *Computer Simulation*, vol. 30, no. 9, pp. 378–381, 2013.

[16] Y. Deshpande, K. Savla, C. Lobo, S. Bhattacharjee, and J. Patel, "Forest monitoring system using sensors, wireless communication and image processing," in *2018 Fourth International Conference on Computing Communication Control and Automation (ICCUBEA)*, 2018, pp. 1–6.

[17] H.-R. Lee, C.-H. Lin, and W.-J. Kim, "Development of an iot-based visitor detection system," in *2016 International SoC Design Conference (ISOCC)*, 2016, pp. 281–282.

[18] S. Bhatia, H. S. Dhillon, and N. Kumar, "Alive human body detection system using an autonomous mobile rescue robot," in *2011 Annual IEEE India Conference*, 2011, pp. 1–5.

[19] G. Lulla, A. Kumar, G. Pole, and G. Deshmukh, "Iot based smart security and surveillance system," in *2021 International Conference on Emerging Smart Computing and Informatics (ESCI)*, 2021, pp. 385–390.

[20] A. Ubaidillah, R. Alfita, and M. S. Wahyudi, "Optimum distance planning of wireless sensor network using linear regression method," in *IOP Conference Series: Materials Science and Engineering*, vol. 1125, no. 1. IOP Publishing, 2021, p. 012072.

[21] M. H. Kefayati, V. Pourahmadi, and H. Aghaeinia, "Wi2vi: Generating video frames from wifi csi samples," *IEEE Sensors Journal*, vol. 20, no. 19, pp. 11 463–11 473, 2020.

[22] Y. Hao, W. Wang, and Q. Lin, "Incident retrieval and recognition in video stream using wi-fi signal," *IEEE Access*, vol. 9, pp. 100 208–100 222, 2021.

[23] M. Lott and I. Forkel, "A multi-wall-and-floor model for indoor radio propagation," in *IEEE VTS 53rd Vehicular Technology Conference, Spring 2001. Proceedings (Cat. No. 01CH37202)*, vol. 1. IEEE, 2001, pp. 464–468.

[24] Y. S. Ku, W. Te Hsu, H. L. Pang, and D. M. Shyu, "System and method for via structure measurement," Mar. 20 2012, uS Patent 8,139,233.

[25] L. Wang, L. Liu, C. Hu, and M. Q.-H. Meng, "A novel rf-based propagation model with tissue absorption for location of the gi tract," in *2010 Annual International Conference of the IEEE Engineering in Medicine and Biology*, 2010, pp. 654–657.

[26] J.-i. Park, Y. Lee, E. Suh, H. Jeon, K.-J. Yoon, and K.-s. Kim, "Improvement of optical flow estimation by using the hampel filter for low-end embedded systems," *IEEE Robotics and Automation Letters*, vol. 6, no. 4, pp. 7233–7239, 2021.